This article has been accepted for publication in a future issue of this journal, but has not been fully edited. Content may change prior to final publication. Citation information: DOI 10.1109/TMECH.2019.2893628, IEEE/ASME Transactions on Mechatronics

Modified repetitive control based cross-coupling compensation approach for a piezoelectric tube scanner of Atomic Force Microscopes

Linlin Li, Chun-Xia Li, Guoying Gu*, and LiMin Zhu

***Abstract*—During the raster scanning of Atomic Force Microscopes (AFMs), the coupling effect from the fast-axis to the slow-axis is extraordinarily pernicious, especially when the scanning rate is set higher. Whilst great efforts have been made in the field of piezo-actuated stages, less attentions are paid on control design to mitigate this coupling effect. In this paper, we propose a modified repetitive control based cross-coupling compensation (MRC-CCC) approach for high-speed and high-precision scanning motion control of a piezoelectric tube scanner in AFMs. Based on the experimental observations, we first describe this coupling effect as the periodic disturbances to the output of the slow-axis, when the fast-axis is designed to track triangular trajectories. Then, the MRC-CCC controller is developed to remedy the periodic disturbances, which generates the compensation signals targeting at coupling effect. Therefore, the complicated modeling of the cross-coupling effect is avoided, which significantly reduces the complexity of usage. To ensure the high-precision tracking performance for the slow-axis in scanning, we further design a tracking controller that combines with the offline trained MRC-CCC controller. Finally, comparative experiments are conducted on a AFM piezoelectric tube scanner. Experimental results show that the developed MRC-CCC approach significantly compensates for the coupling effect, in which the root mean square tracking error is substantially reduced from $172.1nm$ to $3.3nm$ at the scanning rate of 40-Hz. We also perform high-speed scanning tests for AFM imaging to verify the effectiveness of the development.**

***Index Terms*—Atomic force microscope, raster scanning, tracking control, cross-coupling, repetitive control.**

I. Introduction

Since its invention by G. Binner etc [1], [2] in 1986, the Atomic Force Microscope (AFM) has becoming a ubiquitous tool in various research areas in nanoscales [3]–[5]. The basic schematic diagram of the AFM is shown in Fig. 1. The morphology of the sample is recorded by measurement of micro contact forces between the sharp probe and the sample surface via the relative scanning motion. Conventionally, for a commercial AFM, the piezoelectric tube scanner (PTS) [6]–[8] is utilized to fulfill this relative motion with its simple configuration and fine resolution. The widely applied scan trajectory is the back and forth raster pattern, which is attained by applying a triangular trajectory to the X-axis (fast-axis), and the corresponding stair-case trajectory to the Y-axis (slow-axis) shown in Fig. 2(a). The displacements of the X/Y-axis are captured by the integrated capacitive sensors of the piezoelectric scanner, respectively, for closed-loop motion control. As studied in several works [4], [9]–[11], there are many restrictions that hamper the increase of the scanning rate and tracking precision, such as the intrinsic hysteresis nonlinearity of the PTS [12], lightly-damped resonant mode of the mechanism [13], [14], and cross-coupling effect [15]. During the past decades, many efforts have been made to handle the first two challenges above and significant improvements have been achieved [12], [16]–[21]. In these developments, the scanner is generally treated as the single input and single output (SISO) system, in which the cross-coupling effect is not considered.

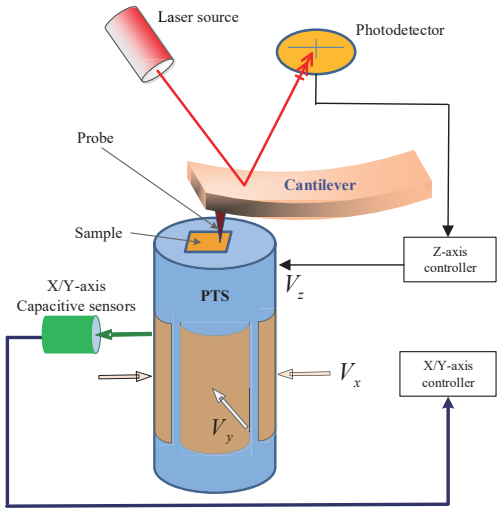

Fig. 1. The schematic diagram of the AFM.

In fact, the cross-coupling effect is gradually becoming the bottleneck that degrades the tracking performance, which is especially prominent in large-range scanning or high-speed operation. Due to the existence of the cross-coupling effect, some tilting phenomenon occurs in the actual scan trajectory, as shown in Fig. 2, which will distort the actual scanning

This work was supported by the National Natural Science Foundation of China under Grant No. 51622506 and the Science and Technology Commission of Shanghai Municipality under Grant No. 16JC1401000. (Corresponding author: Guoying Gu)

L. Li, G. Gu, and L.M. Zhu are with the State Key Laboratory of Mechanical System and Vibration, School of Mechanical Engineering, Shanghai Jiao Tong University, Shanghai 200240, China. (e-mail: lilinlin321@sjtu.edu.cn, guguoying@sjtu.edu.cn, zhulm@sjtu.edu.cn.)

G. Gu is also with Soft Robotics and Biodesign Lab, Robotics Institute, School of Mechanical Engineering, Shanghai Jiao Tong University, Shanghai 200240, China.

C.-X. Li is with KLA-Tencor Corporation, Shanghai 200240, China. (e-mail:lichunxia@sjtu.edu.cn)

This article has been accepted for publication in a future issue of this journal, but has not been fully edited. Content may change prior to final publication. Citation information: DOI 10.1109/TMECH.2019.2893628, IEEE/ASME Transactions on Mechatronics

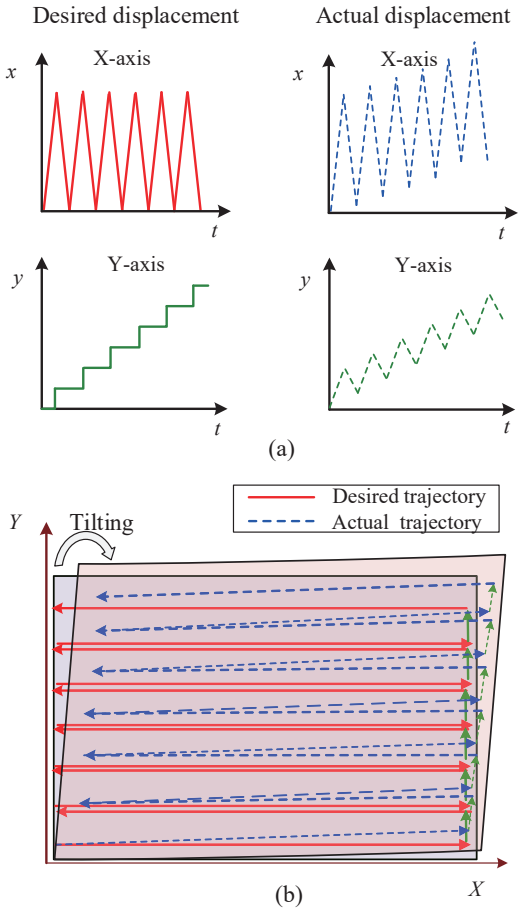

Fig. 2. The diagrammatic representation of cross-coupling effect: (a) the comparison of the desired displacements and actual displacements for X-axis and Y-axis; (b) the comparison of the desired scanning trajectory and the actual scanning trajectory.

trajectory or even swallow the real topography causing artifacts in AFM imaging experiments. To address such challenge, several scanning stages have been designed with symmetric structures to minimize the cross-coupling effect between the axes. However, due to the existence of the machining process errors and the assembling errors, the cross-coupling effect can not be mitigated completely. Although such cross-coupling effect can be ignored at lower scanning frequencies, this effect can still lead to a distorted image or damage of the probe and the sample, specifically when the AFM operates at a higher scanning rate. More importantly, the widely applied PTS presents a much severer cross-coupling effect, which worsens the tracking precision especially for high-speed s-canning. For the objective of reducing the coupling caused tracking errors, some motion control strategies are employed for enhancing the tracking performance, such as the extended robust motion control [22], H_∞ control [23], the adaptive double integral sliding mode control [24]. To further handle the cross-coupling effect, some interesting works, such as neural-network-based coupling model [25], multi-input multi-output model predictive control [15], [26], Prandtl–Ishlinskii model based decoupling control [27], have been reported to compensate this adverse cross-coupling effect. However, due to the complex nonlinear behavior and dynamics of the piezo-actuated stages, the modeling of cross-coupling effect is usually time-consuming and complicated. As an alternative, it is found that the coupling effect from the X-axis mainly affects Y-axis at the harmonics of the input signal in AFM raster scanning pattern, which could be treated as the periodic output disturbances. Then, we propose the modified repetitive controller (MRC) [28] to deal with such challenge without modeling and identification of the cross-coupling dynamics during the raster scanning in this work.

During the raster scanning experiments, the coupling effect from the X-axis to Y-axis commonly much severer than that from the Y-axis to the X-axis. Therefore, this work focuses on the compensation of the coupling effect from the X-axis to Y-axis for raster scanning. According to experimental results in this work, this coupling effect could be deemed as the output periodic disturbances to the system dynamics. Recently, due to its excellent ability of tracking periodic trajectories and rejecting period disturbances, the repetitive control [29]–[33] gains its popularity in the area of piezo-actuated nanopositioning stages, in which the AFM is a typical case. It is known that the repetitive control works via generating high-gains at the harmonics of the desired tracking trajectory. Consequently, it brings the amplification problem of the non-periodic disturbances. For eliminating this issue, the MRC scheme [28] is thus developed. As its better performance, the modified repetitive control based cross-coupling compensation (MRC-CCC) approach is established and implemented on a commercial AFM PTS for high-speed and high-precision raster scanning in this paper. However, the desired scanning trajectory of the Y-axis is the non-periodic stair-case trajectory, which hinders it from being applied successfully. To this end, an offline training method is employed to generate the compensation signal through tracking a constant value signal, in which case, the tracking errors are all introduced by the coupling effect. Then, the captured compensation signal is utilized to alleviate the tracking errors caused by the coupling effect as the feedforward method. For tracking the desired stair-case trajectory, a tracking controller is further incorporated with the offline trained MRC-CCC scheme. The experimental results show that the cross-coupling of the X- and Y- axes are well eliminated with the MRC-CCC approach.

The contribution of this work mainly lies in two aspects:

(1) It is experimentally found that the coupling effect from the X-axis mainly affects the Y-axis at the harmonics of the input signal in AFM raster scanning pattern. This coupling effect is consequently modeled as periodic output disturbances to the dynamics of the Y-axis; In this sense, the MRC scheme is firstly employed to mitigate the cross-coupling effect in the field of piezo-actuated stages, without the modeling and identification of the cross-coupling effect.

(2) For addressing the non-periodic issue of the desired stair-case trajectory in scanning, we develop the offline trained MRC-CCC method combining with a tracking controller, which is also experimentally verified for high-precision and high-speed scanning of piezo-actuated stages.

The remainder of this paper is formulated as follows. Sec .II analyzes the cross-coupling effect in raster scanning. The

This article has been accepted for publication in a future issue of this journal, but has not been fully edited. Content may change prior to final publication. Citation information: DOI 10.1109/TMECH.2019.2893628, IEEE/ASME Transactions on Mechatronics

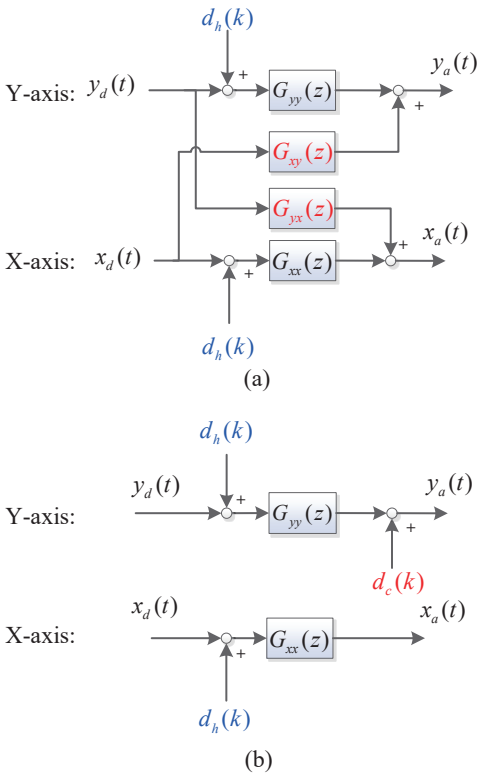

Fig. 3. The dynamics of the system for PTS: (a) the cross-coupling dynamics; (b) the simplified model in raster scanning pattern.

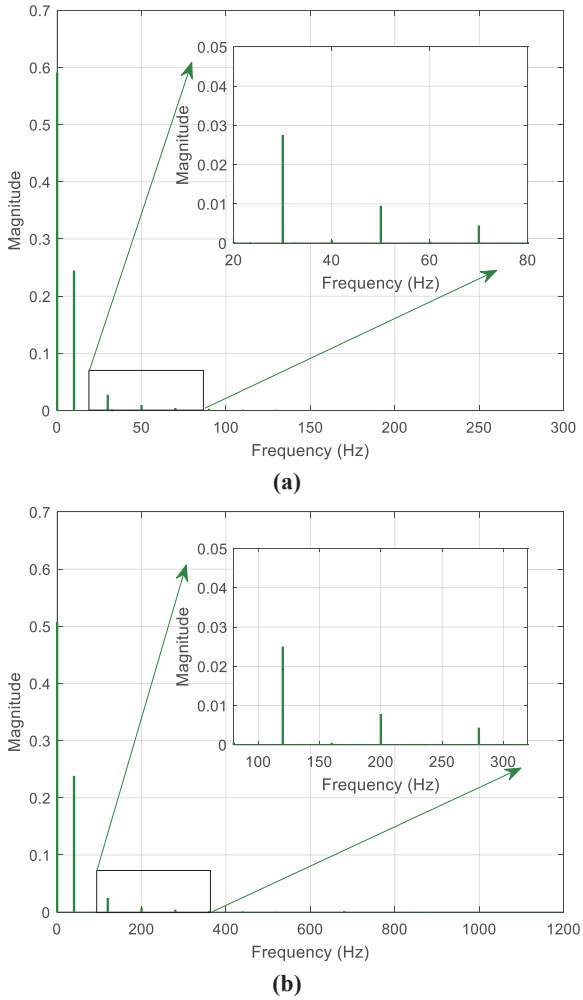

Fig. 4. The spectrogram of the displacement of the Y-axis when the X-axis is tracking triangular trajectory: (a) 10 Hz; (b) 40 Hz.

control schemes for different axes are also presented in this Section. Sec. III illustrates the experimental setup and the experimental results to show the effectiveness of the developed method. The conclusion is summarized in the last section.

II. Problem Statement

A. The cross-coupling effect

In order to accomplish a raster scanning, the X-axis is designed to track a triangular trajectory with a constant frequency, while the Y-axis is set to track a synchronous stair-case signal. However, due to the existence of the cross-coupling effect, the actual scan trajectory distorts severely, as shown in Fig. 2. As a consequence, the tilt will distort the information of the captured image. With the requirement of high-speed and high-precision scanning motion control of the PTS, the cross-coupling effect has to be considered carefully. As discussed in our previous work [28], the hysteresis effect can be treated as periodic disturbances introduced to the input of the system dynamics, when actuated by the periodic control voltage. The block diagram of dynamics for the PTS can thus be described by Fig. 3(a), where $G_{xx}(z)$ and $G_{yy}(z)$ denotes the dynamics of the X- and Y- axes, respectively, $d_h(k)$ is the bounded disturbances introduced by the hysteresis. The $y_d(t)$ and $y_a(t)$ are the desired reference trajectory and the actual output displacement of the Y-axis, respectively. The $x_d(t)$ and $x_a(t)$ are the desired reference trajectory and the actual output displacement of the X-axis, respectively. The term $G_{xy}(z)$ and $G_{yx}(z)$ denotes the cross-coupling dynamics between the X-axis and Y-axis. It is known that the influence from X-axis to Y-axis is much severer than that from the Y-axis to X-axis during the raster scanning. As a result, the coupling effect from the X-axis to Y-axis is captured and investigated in the following. The experiments are performed on a commercial PTS, which is described in the following section.

Taking the scan rate of 10-Hz for example, in such case, the reference input to the X-axis is the triangular signal with the fundamental frequency of 10 Hz. Unlike the stair-case trajectory for Y-axis, the Y-axis is designed to track a constant value in open-loop strategy. It should be noted that the output of the Y-axis is all owing to the coupling effect under this circumstance. The output displacement of the Y-axis is captured and analyzed. By analyzing this signal in frequency domain, the spectra of the output displacement for the Y-axis is shown in Fig. 4(a), for the scanning rate of 10-Hz. It can be found that this coupling effect affects the Y-axis at the fundamental frequency (10 Hz) and the harmonics of the fundamental frequencies (30 Hz, 50 Hz, 70 Hz and so on) of the reference signal to X-axis. Meanwhile, experiments of other scanning rates have also been conducted.

This article has been accepted for publication in a future issue of this journal, but has not been fully edited. Content may change prior to final publication. Citation information: DOI 10.1109/TMECH.2019.2893628, IEEE/ASME Transactions on Mechatronics

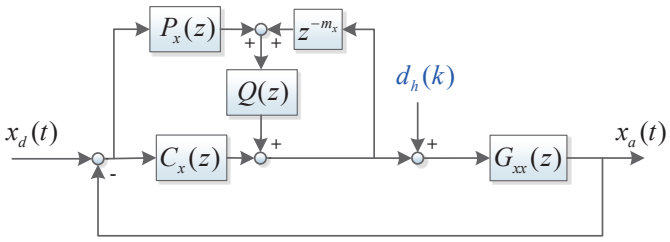

Fig. 5. The block diagram of the MRC scheme for X-axis.

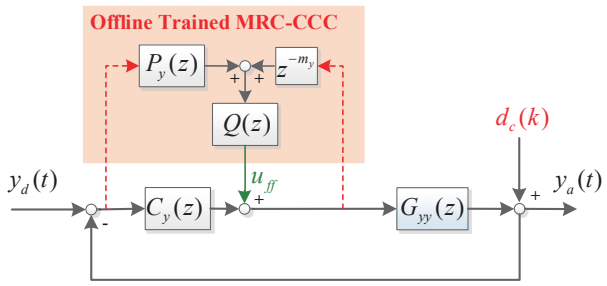

Fig. 6. The block diagram of developed offline trained real-time decoupling method for Y-axis.

These experimental results are consistent with that of the scan rate of 10-Hz. In addition, the spectra of output displacement for the Y-axis with the scanning rate of 40-Hz is illustrated in Fig. 4(b). The output displacement signal of the Y-axis in time domain can be found in Fig. 11 (d) and (f) in open-loop strategy for the scanning rate of 10-Hz and 40-Hz, respectively. For a clear presentation, the enlarged details of Fig. 4 are additionally shown in this figure. Then, we can experimentally conclude that this coupling induced tracking errors can be regarded as the periodic output disturbances to the dynamics of the Y-axis. The coupling dynamics in Fig. 3(a) is thereby simplified to Fig. 3(b) for the PTS in AFM raster scanning pattern, in which the coupling effect from X-axis to Y-axis is represented by $d_c(k)$. As discussed above, the periodic coupling effect can thus be eliminated via the well-designed repetitive control technique during the raster scanning.

B. Controller design

With the objective of achieving high-speed raster scanning with high-precision, the most challenging work is to handle the X-axis and eliminate its effect to Y-axis. For the X-axis, the main limitations are the hysteresis nonlinearity and vibrations resulting from the lightly-damped resonant mode. In [28], [29], it is analyzed that the hysteresis and the vibration caused tracking errors are periodic during the repetition process. Therefore, it is possible that the all these tracking errors can be mitigated by the repetitive control [18], [30], [31], which is an extraordinary work subjected to dealing with the periodic tracking errors and the disturbances [29], [32]. To implement this control method in a discrete time domain and diminish its amplification of the captured noise signal, a MRC approach is utilized to accomplish the triangular trajectory tracking experiments for X-axis, as shown in Fig. 5. The MRC approach introduces a spectrum-selection filter $Q(z)$ to alleviate the non-periodic disturbance amplification problem of the repetitive control. The transfer function of $Q(z)$ is

$$Q(z)=\frac{(1-\beta)z^{-(N-m_x)}}{1-\beta z^{-N}}, \quad \beta \in (0,1) \tag{1}$$

where N is the number of sampling points in one period, and β is determined within experiments to obtain a better noise rejection behavior. For the consideration of stability, an additional low-pass filter $q(z)$ is introduced into the spectrum-selection filter. There are several options available as the low-pass filter, such as $q(z)=(az^{-1}+b+az)^i$ [18] and $q(z)=\frac{c}{z+d}$ [33]. The terms $P_x(z)$ is a the inversion of system dynamics $G_{xx}(z)$, and m_x is the delay determined by the system dynamics and inversion calculation. As a plug-in module, the MRC controller and the tracking controller $C_x(z)$ can be designed independently. For mitigating the residual tracking errors, the widely used proportional and integral (PI) controller is finally chosen as the tracking controller. It should be noted that, due to residual hysteresis nonlinearity and the limited control bandwidth, the imaging data of the ascending slope or the descending slope for the triangular trajectory is commonly collected to establish the topography of the sample. As the zero tracking errors of the triangular trajectory tracking experiments with MRC, it is feasible to generate the sample surface using the data from both ascending slope and the descending slope. In this sense, the total scan time can be shorted by 50%, which is a solution to achieve fast scanning.

For the Y-axis, to achieve the high-precision motion control of the stair-case trajectory, the most challenging problem is the coupling effect from X-axis. According to the analysis in the previous part, the MRC control approach is capable of dealing with the periodic output disturbances introduced by coupling effect. However, on account of the aperiodicity of the stair-case signal (in Fig. 2(a)), the MRC control approach is not applicable in this case. For handling this issue, the Y-axis is designed to track a constant value at first, the periodic tracking errors caused by the coupling effect can be eliminated with the MRC approach. Therefore, the offline trained MRC-CCC approach is developed to generate the compensation signal $u_{ff}(t)$, which acts as the feedforward method in real-time scanning. The block diagram of developed offline trained real-time decoupling method is shown in Fig. 6, where the basic control idea are same with that in Fig. 5. Due to the low variation of the stair-case trajectory, the hysteresis induced input disturbances $d_h(k)$ are ignored in this control diagram. For training the compensation signal, the desired trajectory $y_d(t)$ in Fig. 6 is set as 0 as an illustration. On this condition, all the compensation voltage $u_{ff}(t)$ for trajectories with different scan rates can be captured and recorded. Incorporated with the tracking control $C_y(z)$, the MRC-CCC approach can be designed to realize the tracking experiments of the stair-case trajectory. For convenience, the tracking controller is also determined as the PI controller. It is worthy of mentioning that when the Y-axis is configured to track a constant value, the tracking errors are all owing to coupling effect, and the captured compensation signal is only aimed to mitigate this

This article has been accepted for publication in a future issue of this journal, but has not been fully edited. Content may change prior to final publication. Citation information: DOI 10.1109/TMECH.2019.2893628, IEEE/ASME Transactions on Mechatronics

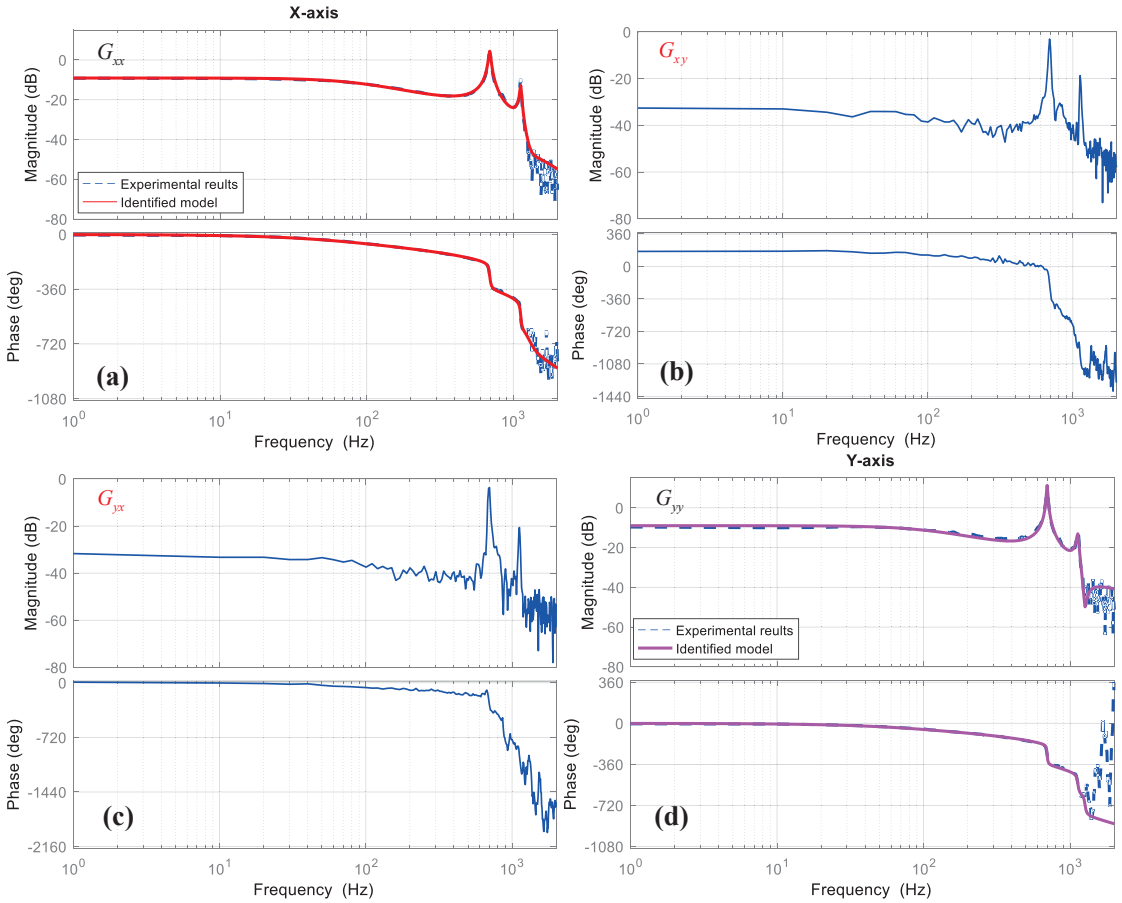

Fig. 8. The identified frequency responses: (a) X-axis; (b) the coupling dynamics from X-axis to Y-axis; (c) the coupling dynamics from Y-axis to X-axis; (d) Y-axis.

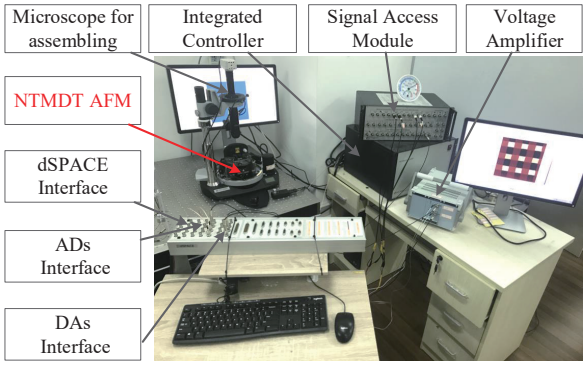

Fig. 7. The experimental setup.

coupling effect.

III. Experimental Studies

In this section, the experimental setup and the detailed information of the MRC-CCC approach is presented. Besides, the tracking performance of the PTS and its imaging application in AFM are illustrated to show the effectiveness of the developments on decoupling control, compared with the pure tracking controller.

A. Experimental setup

To validate the effectiveness of the developed control method, an AFM designed by NTMDT company is used in this work. The overall experimental setup is shown in Fig. 7. This setup consists of three main parts: the AFM system to realize the scan motion and establish the topography of the sample surface, the dSPACE to implement the control approaches, and the voltage amplifier to generate the actuation voltage for the scanner. The AFM system is composed of the scan module, the signal access module, an integrated controller and a microscope assisting for mounting the sample and probe. The scan module adopted in this work is the head scanner, which means that the relative scanning motion is obtained via the movement of the probe. This scanner can achieve the movements in X-Y-Z directions simultaneously. Each axis is equipped with a capacitive sensor for capturing the actual displacement signals. The travel range of the scanner is $100um \times 100um \times 10um$. To implement the control approaches, the dSPACE DS-1103 is configured, which has an interface with 16-bit ADs and 16-bit DAs. The 16-bit ADs can capture the analog displacement signal from the capacitive sensors via the integrated controller and transfer it to the dSPACE host as digital signals. At the same time, the digital signal processing is in process within dSPACE host to fulfill the closed-loop control. The 16-bit DAs are utilized to deliver the control voltages to the high-voltage

This article has been accepted for publication in a future issue of this journal, but has not been fully edited. Content may change prior to final publication. Citation information: DOI 10.1109/TMECH.2019.2893628, IEEE/ASME Transactions on Mechatronics

amplifier. The voltage amplifier with the amplification factor of 30 is utilized to provide the high-voltage signals to the PTS for actuation. For illustrating the effectiveness of the decoupling performance of the proposed method with AFM images, the constant height mode is set. The high resolution contact probe CSG01 from NTMDT is configured, where the resonance is 9.8 kHz and the force constant is 0.03 N/m. The TGQ1 grating sample from NTMDT is utilized with square microstucture, whose period is $3\mu m$. The sampling frequency of the dSPACE control board is set to be 10 kHz.

B. The controller implementation

For the objective of designing the MRC scheme for X-axis and MRC-CCC scheme for Y-axis, the dynamics of these two systems have to be identified at first. To this end, the band-limited white noise signal with low amplitude is generated to excite one of these two axes (X/Y-axis), in which the other axis (Y/X-axis) is designed to track a constant value in open-loop strategy. The input noise signal and the output displacement signal are captured simultaneously, which are utilized to determine the dynamics of the X-axis and Y-axis with the Matlab Identification Toolbox. The identified transfer functions of the X-axis and Y-axis are expressed as

$$G_{xx}(z) = z^{-1}\frac{0.001z^5-0.0003z^4+0.002z^3-0.003z^2-0.004z+0.003}{z^6-4.347z^5+8.206z^4-8.409z^3+4.762z^2-1.293z+0.8583} \tag{2}$$

$$G_{yy}(z) = z^{-1}\frac{0.008z^4-0.030z^3+0.050z^2-0.041z+0.015}{z^5-4.234z^4+7.749z^3-7.601z^2+3.995z-0.9024} \tag{3}$$

The comparison of the experimental results and the identified model is shown in Fig. 8(a) and Fig. 8(d), respectively. As can be observed in this figure, the identified model could describe the system dynamics precisely. Furthermore, the cross-coupling dynamics between these two axes are presented as well, where the severe cross-coupling effect can be observed clearly.

Take Y-axis for instance, it is convenient to deduce the parameters of the MRC-CCC scheme with the identified dynamics. From Eq. (3), it can be calculated that this system is a non-minimum phase system. Stemming from this fact, a zero-phase-tracking-control method [34] is employed to acquire the model inversion of the Y-axis. Therefore,

$$P_y(z) = \frac{A(z)}{B(z)} = z^{-(mu+mc)}\frac{A(z)B_f(z)}{B_s(z)[B_u(1)]^2} \tag{4}$$

where $A(z)$ and $B(z)$ are the denominator and the nominator of transfer function of the Y-axis, the $B_s(z)$ is composed of all the stable zeros, $B_u(z)$ is composed of all the unstable zeros and $B_f(z)$ is obtained via flipping the coefficients of $B_u(z)$. The parameter mu is the number of the unstable zeros and mc is the compensation term to keep the system inversion causal. The delayed steps m_y is the sum of the identified delays and the parameter mc. According to Eq. 3, there exists four unstable zeros, and thus the order to system inversion casual is calculated as 5. Therefore, the delayed steps m_y is thus computed as 6. Similarly, the delayed steps m_x for X-axis is computed as 7. On account of the performance of

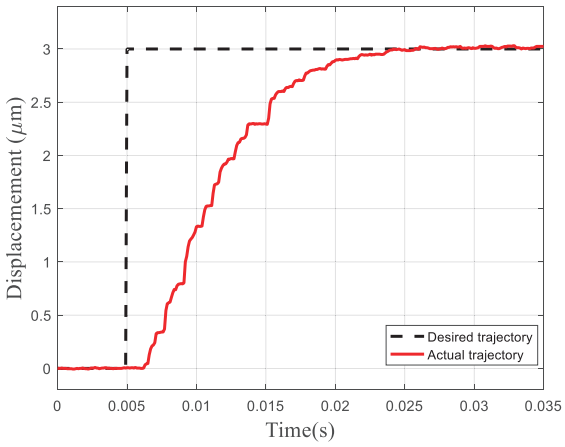

Fig. 9. The step response of the Y-axis with PI control.

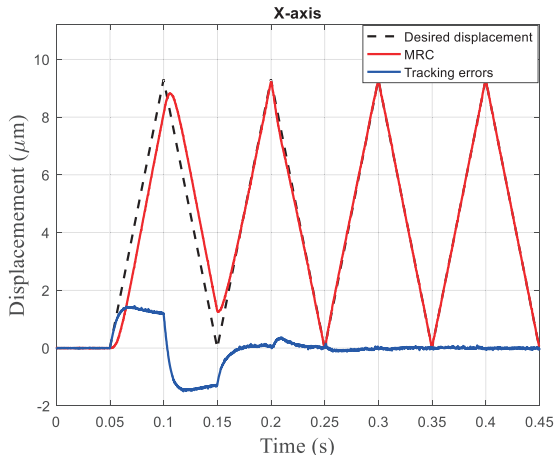

Fig. 10. The convergence experimental results of X-axis with varying β for the scanning rate of 10-Hz.

the filter and the bandwidth of the system, the low pass filter in $Q(z)$ is determined to be $q(z)=(az^{-1}+b+az)^i$, where $a = 0.25,\ b = 0.5, i = 6$. It is known that the higher the control gain is, the better the tracking performance is for the system with PI control. However, the higher control gains may cause low relative stability margin [14]. Hence, the control gains are finally maximized before the vibration occurs for the step response, which is plotted in Fig. 9. The slightly vibration can be observed in this figure. The control gains of PI control are finally determined as $k_p = 0.01, k_i = 350$ for the Y-axis, with trial and error method in experiments.

To optimize the parameter β, the convergence experiments are performed. It should be noted that when the parameter β is set to 0, the MRC scheme is converted to the traditional repetitive control, which requires the shortest convergence time. Based on the convergence experimental results, it can be found that the repetitive control in this work requires approximately two scanning cycles before convergence for X- and Y- axes. Since the MRC-CCC for Y-axis is trained offline, the convergence time is not an issue for real-time AFM scanning. Therefore, the convergence experiments for X-axis are studied here. To make a balance between the convergence speed and the noise rejection property, the parameter β in $Q(z)$

This article has been accepted for publication in a future issue of this journal, but has not been fully edited. Content may change prior to final publication. Citation information: DOI 10.1109/TMECH.2019.2893628, IEEE/ASME Transactions on Mechatronics

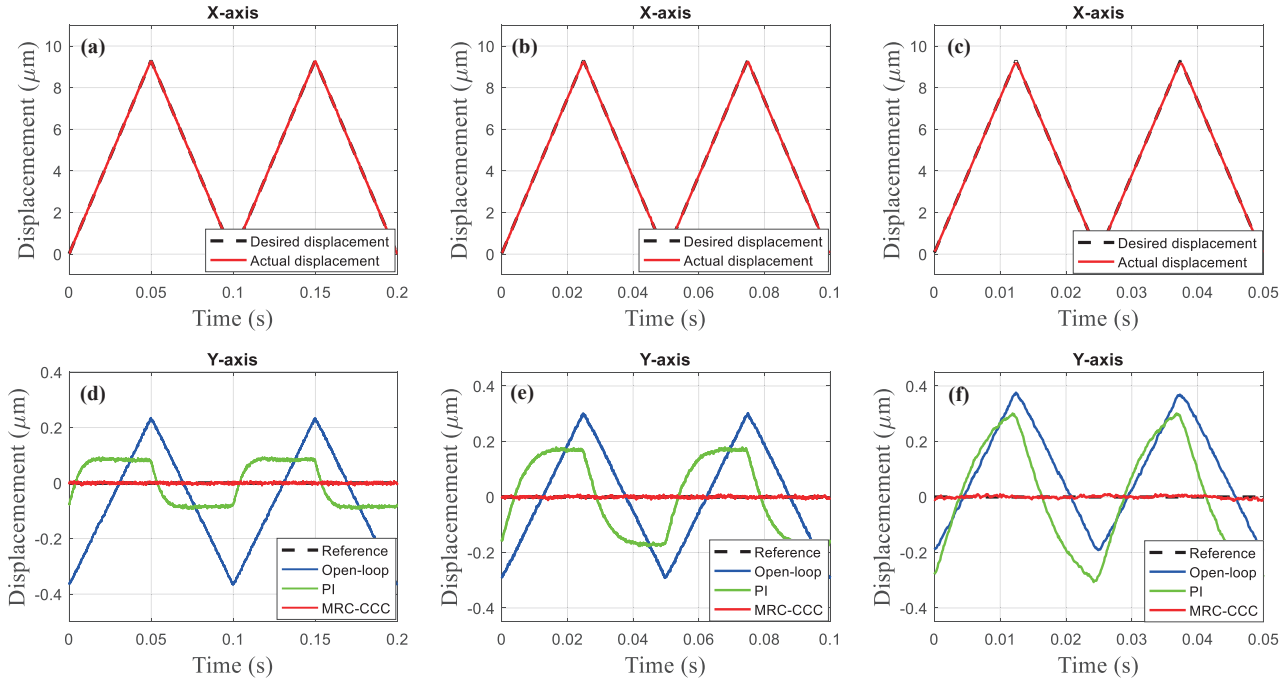

Fig. 11. Experimental results: (a)-(c) The triangular trajectory tracking results of the X-axis for the frequency of 10-Hz, 20-Hz, 40-Hz, respectively; (d)-(f) The coupling induced tracking results the Y-axis for the frequency of 10-Hz, 20-Hz, 40-Hz, respectively, under different control methods.

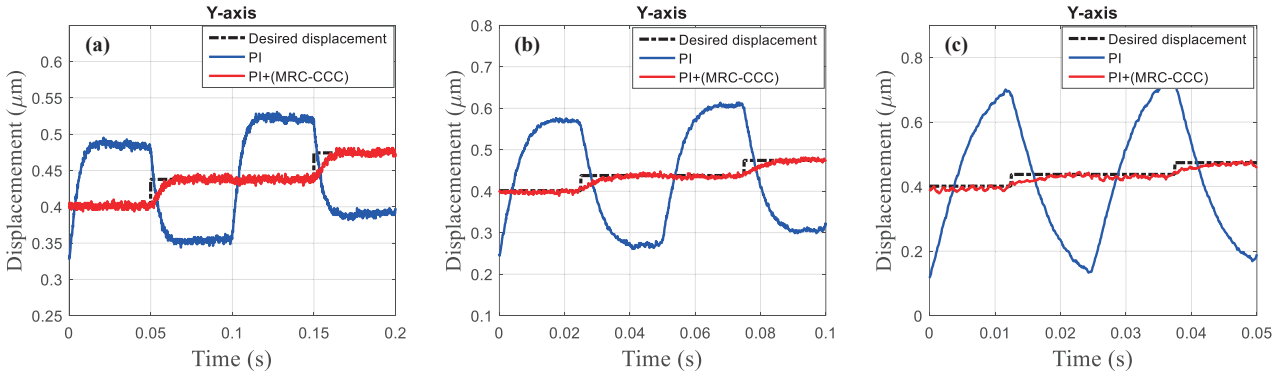

Fig. 12. The tracking results of the Y-axis with different control methods for different scanning rates: (a) 10 Hz; (b) 20 Hz; (c) 40 Hz.

is set as 0 during the first two periods, where the MRC scheme is simplified to the traditional repetitive control approach, and increase to 0.9 incrementally in the next two scanning cycles. Take the scanning rate of 10-Hz for illustration, the convergence experimental results with varying β for X-axis are shown in Fig. 10, where the shortest convergence time is also achieved. This varying parameter method is employed for MRC-CCC scheme of Y-axis as well. With all the parameters determined, the experimental results are presented in the following part. Note that, to guarantee the decoupling performance, the coupling compensation signals are captured after several iterative cycles. For more information of the MRC scheme and the parameters optimization, readers can refer to [28].

Remark 1. *As for the MRC scheme of X-axis in real-time AFM scanning experiments, it requires at least two scanning cycles to converge, during which the tracking precision is not high enough for scanning. In this work, before the convergence of the X-axis, the Y-axis is designed to track a constant value, and these two scanning cycles are abandoned in imaging experiments.*

C. Experimental tracking results of the PTS

As analyzed in Sec. II, this section presents the experimental results to show the effectiveness of the MRC-CCC approach on coupling compensation. Since the tracking controller is the widely used PI controller, the comparative experiments for Y-axis with MRC-CCC control is set as pure PI controller to track a constant value, where the gains of the PI controller for Y-axis with PI control and Y-axis with MRC-CCC control are the same. For all comparative experiments, the X-axis is designed to track the triangular trajectory with the PI+MRC scheme.

The 10-Hz tracking results of the X-axis with PI+MRC is shown in Fig. 11(a). It can be observed that with the PI+MRC

This article has been accepted for publication in a future issue of this journal, but has not been fully edited. Content may change prior to final publication. Citation information: DOI 10.1109/TMECH.2019.2893628, IEEE/ASME Transactions on Mechatronics

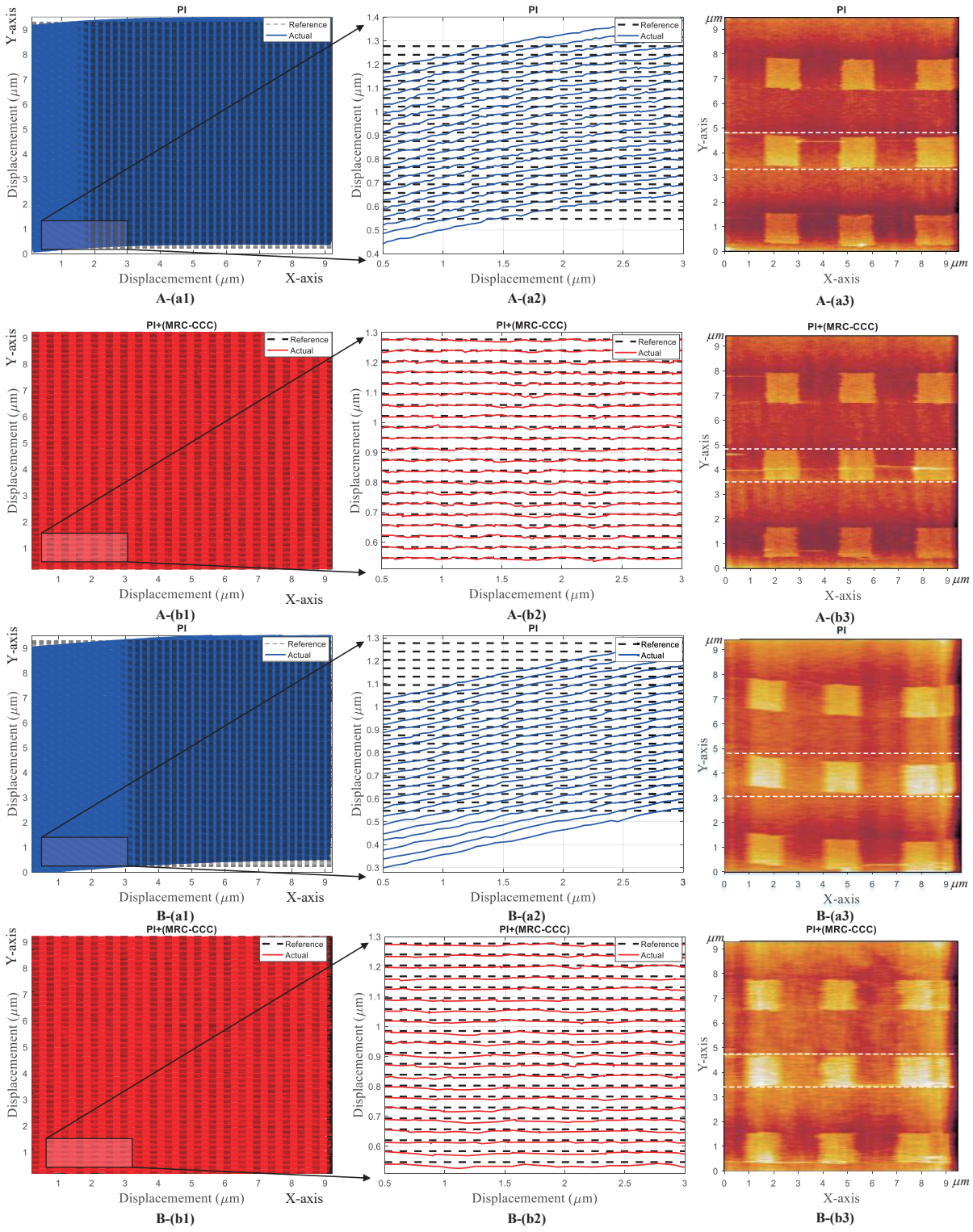

Fig. 13. The scanning experimental results for different control methods with different scanning rates: (A) 20-Hz; (B) 40-Hz; (a) The experimental results for PI control; (b) The experimental results results for PI+(MRC-CCC) control; (1) The comparison of the desired scanning trajectory with the actual scanning trajectory; (2) The enlarged details of the comparative results; (3) The corresponding AFM image.

scheme, the X-axis tracks the desired triangular trajectory accurately. The tracking results of the Y-axis in open-loop strategy, with PI control, and with MRC-CCC control are also illustrated in this figure, which are all design to tracking a constant value. It is worthy of mentioning that the tracking errors of Y-axis all result from the coupling effect at this case. It can be seen from Fig. 11(d) that due to the existence of the coupling effect, it is tough for the PI controller to track the desired trajectory accurately, though the tracking frequency of X-axis is only 10 Hz. In addition, the 20 Hz

This article has been accepted for publication in a future issue of this journal, but has not been fully edited. Content may change prior to final publication. Citation information: DOI 10.1109/TMECH.2019.2893628, IEEE/ASME Transactions on Mechatronics

and 40-Hz tracking results for the X-axis and Y-axis with different control approaches are shown in Fig. 11(b),(e) and Fig. 11(c),(f), respectively. Comparing these figures, it can be found that with the increase of the tracking frequency, the PI controller is not capable of compensating the coupling effect, especially for the frequency of 40 Hz shown in Fig. 11(f). It is because of the high-frequency components involved in the coupling effect and the limited control bandwidth of the PI controller that the Y-axis with pure PI control failed to track the desired displacement. From Fig. 11(f), it can be seen noticeably that the coupling amplitude for Y-axis with PI control is approximately equal to that in open-loop strategy, while the Y-axis with MRC-CCC control is kept in excellent tracking performance. It should be noted that the compensation signals for mitigating the coupling effect in Fig. 11(d),(e),(f) of MRC-CCC control are captured and recorded as the offline trained MRC-CCC controller, which verifies the accuracy of the development.

For quantitatively comparing the tracking performance of the Y axis with different control approaches, the maximum tracking errors e_m and the root mean square tracking errors e_{rms} , defined as

$$e_m = \max_{t\in(0,2T]} |y_a(t) - y_d(t)| \tag{5}$$

$$e_{rms} = \sqrt{\frac{1}{2T}\int_0^{2T} [y_d(t) - y_a(t)]^2} \tag{6}$$

are summarized in Table I, where T is the period of the input signals to X-axis. By comparison, for the frequency of 40 Hz, the root mean square tracking errors with MRC-CCC control is reduced from $172.1nm$ to $3.3nm$. On contrary, the tracking errors with PI control is almost equal to that in open-loop, which is even larger than the scanning resolution. On the basis of the above-mentioned results, it is concluded that the developed MRC-CCC technique exhibits excellent performance on compensation of the coupling effect.

TABLE I
TRACKING ERRORS OF THE Y-AXIS WITH DIFFERENT CONTROL APPROACHES FOR DIFFERENT FREQUENCIES OF THE X-AXIS.

Frequency(Hz)	Open-loop (μm)		PI (μm)		MRC-CCC (μm)	
	e_m	e_{rms}	e_m	e_{rms}	e_m	e_{rms}
10	0.3064	0.1746	0.0954	0.0777	0.0095	0.0027
20	0.3256	0.1754	0.1790	0.1368	0.0095	0.0029
40	0.3146	0.1721	0.3033	0.1981	0.0118	0.0033

D. Imaging application in AFM

The foremost control objective of this work is to minimize the tracking errors during raster scanning. Hence, the raster trajectory tracking tests are performed on the AFM described in Sec. III-A. For achieving the stair-case trajectory tracking experiments, an additional PI controller is incorporated with the offline-trained MRC-CCC controller as shown in Fig. 6. As mentioned above, the X-axis is also design with the PI+MRC scheme for tracking the triangular trajectory. The Y-axis is corresponding designed to track the stair-case trajectory with different control approaches, which are the PI+(MRC-CCC) control and the PI control for comparison. The tracking results of the Y-axis for different control methods with different scanning rates are shown in Fig. 12. As shown in this figure, in comparison with the PI controller, the PI+(MRC-CCC) control method improves the tracking performance of the Y-axis for the stair-case trajectory significantly, even in high-speed scanning. This experimental results validate the effectiveness and suitability of the developed method on mitigating the coupling effect in AFM scanning experiments, where the PI controller deals with the trajectory variation of the Y-axis and other disturbances, the offline trained MRC-CCC controller deals with the coupling effect. The raster trajectory tracking results for different control methods with different scanning rates are presented in Fig. 13(1). The enlarged details are also presented in this figure, where only the selected desired scanning trajectory and the actual scanning trajectory are plotted. It can be seen from Fig. 13 that, due to the tracking errors induced by coupling effect, the raster scan trajectory appears severe trajectory distortion, which will consequently result in artifacts or image distortion. For the convenience of understanding, the AFM image are additionally illustrated in Fig. 13(3), where the experimental results of the system with PI+(MRC-CCC) control and with PI control are presented corresponding to the scanning trajectory. Note that due to the digital signal process in capturing the height signal, the imaging resolution for the scanning rate of 20-Hz and 40-Hz are 250×250 and 250×125, respectively. With PI control, the image distortion can be observed clearly from Fig. 13A-(a3) and B-(a3), where the microstructure of square is shaped to deformed rhombus pronouncedly. In contrast, with PI+(MRC-CCC) control, the problem caused by the coupling effect is well handled, as shown in Fig. 13A-(b3) and B-(b3). Even though the excellent decoupling performance, the raster scan tests are not performed with a higher frequency (more than 40-Hz), in consideration of the limited bandwidth of the Z-axis, where the captured image with higher scanning rate is not so clear as that with a lower one.

IV. CONCLUSION

In this paper, a MRC-CCC approach is proposed and verified on a PTS of AFM for fast raster scanning with high-precision. The development lies in the fact that the coupling effect can be analyzed as the periodic output disturbances to the system dynamics during repetition operation. Therefore, the complicated modeling and identification of the cross-coupling dynamics is avoided for the development, which significantly lower the implementation complexity. As the raster trajectory for the Y-axis is non-periodic, the offline trained MRC-CCC approach is employed to generate the compensation signals, which acts as feedforward controller to mitigate the influence caused by the coupling effect. For realizing the raster scanning, the developed MRC-CCC controller is combined with the PI controller for tracking the stair-case trajectories of the Y-axis. Experimental results show that the developed control method is effective on tracking the stair-case trajectory with the scanning rate up to 40-Hz, where the coupling effect caused tracking errors are reduced prominently.

REFERENCES

[1] G. Binnig, C. F. Quate, and C. Gerber, Atomic force microscope, *Phys. Rev. Lett.*, vol. 56, no. 9, pp.930-933, 1986.

[2] S. Salapaka and M. Salapaka, Scanning Probe Microscopy, *IEEE Control Syst. Mag.*, vol. 28, no. 2, pp. 65–83, Apr. 2008.

[3] T. Uchihashi, R. Iino, T. Ando, and H. Noji, High-Speed Atomic Force Microscopy Reveals Rotary Catalysis of Rotorless F1-ATPase, *Science*, vol. 333, no. 6043, p. 755, Aug. 2011.

[4] M. S. Rana, H. R. Pota, and I. R. Petersen, Improvement in the Imaging Performance of Atomic Force Microscopy: A Survey, *IEEE Trans. Autom. Sci. Eng.*, vol. 14, no. 2, pp. 1265–1285, Apr. 2017.

[5] Y. F. Dufrêne, T. Ando, R. Garcia, et al, Imaging modes of atomic force microscopy for application in molecular and cell biology. *Nat. Nanotechnol*, vol. 12, no. 4, pp. 295–307, 2017.

[6] G. Schitter and A. Stemmer, Identification and Open-Loop Tracking Control of a Piezoelectric Tube Scanner for High-Speed Scanning-Probe Microscopy, *IEEE Trans. Control Syst. Technol.*, vol. 12, no. 3, pp. 449–454, 2004.

[7] B. Bhikkaji, M. Ratnam, A. J. Fleming, and S. O. R. Moheimani, High-Performance Control of Piezoelectric Tube Scanners, *IEEE Trans. Control Syst. Technol.*, vol. 15, no. 5, pp. 853–866, 2007.

[8] M. S. Rana, H. R. Pota, and I. R. Petersen, A Survey of Methods Used to Control Piezoelectric Tube Scanners in High-Speed AFM Imaging, *Asian J. Control*, 2018.

[9] G.-Y. Gu, L.-M. Zhu, C.-Y. Su, H. Ding, and S. Fatikow, Modeling and Control of Piezo-Actuated Nanopositioning Stages: A Survey, *IEEE Trans. Autom. Sci. Eng.*, vol. 13, no. 1, pp. 313–332, 2016.

[10] Z. Li and J. Shan, Inverse Compensation Based Synchronization Control of the Piezo-Actuated Fabry–Perot Spectrometer, *IEEE Trans. Ind. Electron.*, vol. 64, no. 11, pp. 8588–8597, 2017.

[11] Z. Li and J. Shan, Modeling and Inverse Compensation for Coupled Hysteresis in Piezo-Actuated Fabry–Perot Spectrometer, *IEEE/ASME Trans. Mechatron.*, vol. 22, no. 4, pp. 1903–1913, 2017.

[12] P.-K. Wong, Q. Xu, C.-M. Vong, and H.-C. Wong, Rate-Dependent Hysteresis Modeling and Control of a Piezostage Using Online Support Vector Machine and Relevance Vector Machine, *IEEE Trans. Ind. Electron.*, vol. 59, no. 4, pp. 1988–2001, 2012.

[13] A. J. Fleming, Nanopositioning System With Force Feedback for High-Performance Tracking and Vibration Control, *IEEE/ASME Trans. Mechatron.*, vol. 15, no. 3, pp. 433-447, 2010.

[14] L. Li, C.-X. Li, G. Gu, and L.-M. Zhu, Positive acceleration, velocity and position feedback based damping control approach for piezo-actuated nanopositioning stages, *Mechatronics*, vol. 47, pp. 97–104, 2017.

[15] M. S. Rana, H. R. Pota, and I. R. Petersen, Nonlinearity Effects Reduction of an AFM Piezoelectric Tube Scanner Using MIMO MPC, *IEEE/ASME Trans. Mechatron.*, vol. 20, no. 3, pp. 1458–1469, 2015.

[16] G.-Y. Gu and L.-M. Zhu, Motion control of piezoceramic actuators with creep, hysteresis and vibration compensation, *Sens. Actuators Phys.*, vol. 197, pp. 76–87, 2013.

[17] V. Hassani, T. Tjahjowidodo, and T. N. Do, A survey on hysteresis modeling, identification and control, *Mech. Syst. Signal Process.*, vol. 49, no. 1–2, pp. 209–233, 2014.

[18] C.-Y. Lin and P.-Y. Chen, Precision tracking control of a biaxial piezo stage using repetitive control and double-feedforward compensation, *Mechatronics*, vol. 21, no. 1, pp. 239–249, 2011.

[19] M. S. Rana, H. R. Pota, and I. R. Petersen, Performance of Sinusoidal Scanning With MPC in AFM Imaging, *IEEE/ASME Trans. Mechatron.*, vol. 20, no. 1, pp. 73–83, 2015.

[20] Y. Qin, Y. Tian, D. Zhang, B. Shirinzadeh, and S. Fatikow, A Novel Direct Inverse Modeling Approach for Hysteresis Compensation of Piezoelectric Actuator in Feedforward Applications, *IEEE/ASME Trans. Mechatron.*, vol. 18, no. 3, pp. 981–989, Jun. 2013.

[21] G. M. Clayton, S. Tien, K. K. Leang, Q. Zou, and S. Devasia, A Review of Feedforward Control Approaches in Nanopositioning for High-Speed SPM, *J. Dyn. Syst. Meas. Control*, vol. 131, no. 6, p. 061101, 2009.

[22] U. Bhagat, B. Shirinzadeh, L. Clark, Y. Qin, Y. Tian, and D. Zhang, Experimental Investigation of Robust Motion Tracking Control for a 2-DOF Flexure-Based Mechanism, *IEEE/ASME Trans. Mechatron.*, vol. 19, no. 6, pp. 1737–1745, 2014.

[23] Y. K. Yong, K. Liu, and S. O. R. Moheimani, Reducing Cross-Coupling in a Compliant XY Nanopositioner for Fast and Accurate Raster Scanning, *IEEE Trans. Control Syst. Technol.*, vol. 18, no. 5, pp. 1172–1179, 2010.

[24] J. Wu, J. Chen, M. Chiang, J. Yu and L. Fu, Design and Control of Phase-Detection Mode Atomic Force Microscopy for Reconstruction of Cell Contours in Three Dimensions," *IEEE Trans. Nanotechnol.*, vol. 13, no. 4, pp. 639-649, 2014.

[25] Y. Xie, Y. Tan and R. Dong, Nonlinear Modeling and Decoupling Control of XY Micropositioning Stages With Piezoelectric Actuators, *IEEE/ASME Trans. Mechatron.*, vol. 18, no. 3, pp. 821-832, 2013.

[26] S. K. Das, H. R. Pota, and I. R. Petersen, Multivariable Negative-Imaginary Controller Design for Damping and Cross Coupling Reduction of Nanopositioners: A Reference Model Matching Approach, *IEEE/ASME Trans. Mechatron.*, vol. 20, no. 6, pp. 3123–3134, 2015.

[27] Z. Guo, Y. Tian, X. Liu, B. Shirinzadeh, F. Wang, D. Zhang, An inverse Prandtl–Ishlinskii model based decoupling control methodology for a 3-DOF flexure-based mechanism, *Sensors and Actuators A: Physical*, vol. 230, pp. 52-62, 2015.

[28] C.-X. Li, G.-Y. Gu, M.-J. Yang, and L.-M. Zhu, High-Speed Tracking of a Nanopositioning Stage Using Modified Repetitive Control, *IEEE Trans. Autom. Sci. Eng.*, vol. 14, no. 3, pp. 1467–1477, 2017.

[29] U. Aridogan, Y. Shan, and K. K. Leang, Design and Analysis of Discrete-Time Repetitive Control for Scanning Probe Microscopes, *RJ. Dyn. Syst. Meas. Control*, vol. 131, no. 6, p. 061103, 2009.

[30] X. Chen and M. Tomizuka, New Repetitive Control With Improved Steady-State Performance and Accelerated Transient, *IEEE Trans. Control Syst. Technol.*, vol. 22, no. 2, pp. 664–675, Mar. 2014.

[31] A. A. Eielsen, J. T. Gravdahl, and K. K. Leang, Low-order continuous-time robust repetitive control: Application in nanopositioning, *Mechatronics*, vol. 30, pp. 231–243, 2015.

[32] M. Tomizuka, T.-C. Tsao, and K.-K. Chew, Analysis and Synthesis of Discrete-Time Repetitive Controllers, *J. Dyn. Syst. Meas. Control*, vol. 111, no. 3, pp. 353–358, 1989.

[33] Y. Shan and K. K. Leang, Accounting for hysteresis in repetitive control design: Nanopositioning example, *Automatica*, vol. 48, no. 8, pp. 1751–1758, 2012.

[34] J. A. Butterworth, L. Y. Pao, and D. Y. Abramovitch, Analysis and comparison of three discrete-time feedforward model-inverse control techniques for nonminimum-phase systems, *Mechatronics*, vol. 22, no. 5, pp. 577–587, 2012.

Linlin Li received the B.E. degree (with honors) in mechanical design, manufacturing, and automation from Shandong University, Jinan, China, in 2014. She is currently working toward the Ph.D. degree in mechanical engineering at Shanghai Jiao Tong University, Shanghai, China.

Her research interests include mechatronics, modeling and control of high-bandwidth nanopositioning stages, and atomic force microscope.

Chun-Xia Li (S'12) received the B.E. degree (with honors) and the Ph.D. degree (with honors) in mechanical engineering from Shanghai Jiao Tong University, Shanghai, China, in 2011 and 2017, respectively. She is currently working at the KLA-Tencor Corporation, in Shanghai, China.

Dr. Li was the recipient of the National Scholarship for Excellent Master/Doctoral Student granted by Ministry of Education of China in 2012 and in 2016, respectively.

Guoying Gu (S'10-M'13) received the B.E. degree (with honors) in electronic science and technology, and the Ph.D. degree (with honors) in mechatronic engineering from Shanghai Jiao Tong University, Shanghai, China, in 2006 and 2012, respectively.

Since October 2012, Dr. Gu has worked at Shanghai Jiao Tong University, where he is currently appointed as a Professor of School of Mechanical Engineering. He was a Humboldt Postdoc Fellow with University of Oldenburg, Oldenburg, Germany. He was a Visiting Scholar with Massachusetts Institute of Technology, National University of Singapore, and Concordia University. His research interests include soft robotics, bioinspired robot design and motion control, smart materials actuators and sensors, and additive manufacturing with soft materials. He is the author or co-author of over 70 publications, which have appeared in journals, as book chapters and in conference proceedings.

Dr. Gu is the winner of multiple wards including Young Changjiang Scholar of the Ministry of Education, National Science Fund for Excellent Young Scholars, The first prize of natural science of Ministry of Education, Best Paper Award at the 2016 International Conference on Intelligent Robotics and Applications and 2011 IEEE International Conference on Information and Automation. He is a member of the IEEE and ASME. Now he serves as Associate Editor of International Journal of Advanced Robotic Systems. He has also served for several international conferences/symposiums as Chair, Associate Editor or Program Committee Member.

LiMin Zhu received the B.E. degree (with honors) and the Ph.D. degree in mechanical engineering from Southeast University in 1994 and 1999, respectively. From Nov. 1999 to Jan. 2002, he worked as a postdoctoral fellow in Huazhong University of Science and Technology. Since March 2002, he has been with Shanghai Jiao Tong University, where he is currently the "Cheung Kong" Chair Professor, head of the Department of Mechanical Engineering and vice director of the State Key Laboratory of Mechanical System and Vibration. He has held the visitorship in Monash University (from Sep. 1997 to May 1998) and The City University of Hong Kong (from Dec. 2000 to Mar. 2001). His research interests include (1) Multi-axis CNC machining technology and machine tool, (2) coordinate metrology and measurement, and (3) control, sensing and instrumentation for micro/nano manufacturing. He has published 1 monograph and more than 150 international journal papers.

Prof. Zhu was the recipient of the National Science Fund for Distinguished Young Scholars in 2013 and selected into the National High-level Personnel of Special Support Program in 2016. He has been an Associate Editor for the IEEE Transactions on Automation Science and Engineering. He is now a Technical Editor for the IEEE/ASME Transactions on Mechatronics, and Editorial Board Members of the Proceedings of the Institution of Mechanical Engineer (IMechE), Part B: Journal of Engineering Manufacture, and Chinese Journal of Mechanical Engineering.